

Nanotube caps on Ni, Fe, and NiFe nano particles: A path to chirality selective growth

Heiko Dumlich,[†] John Robertson,[‡] and Stephanie Reich^{*,†}

Fachbereich Physik, Freie Universität Berlin, 14195 Berlin, Germany, and Department of Engineering, University of Cambridge, Cambridge CB2 1PZ, United Kingdom

E-mail: reich@physik.fu-berlin.de

Abstract

Carbon nanotubes have properties depending on the arrangement of carbon atoms on the tube walls, called chirality. Also it has been tried to grow nanotubes of only one chirality for more than a decade it is still not possible today. A narrowing of the distribution of chiralities, however, which is a first step towards chirality control, has been observed for the growth of nanotubes on catalysts composed of nickel and iron. In this paper, we have calculated carbon-metal bond energies, adhesion energies and charge distributions of carbon nanotube caps on Ni, Fe and NiFe alloy clusters using density functional theory. A growth model using the calculated energies was able to reproduce the experimental data of the nanotube growth on the alloy catalysts. The electronic charge was found to be redistributed from the catalyst particles to the edges of the nanotube caps in dependence of the chiral angles of the caps increasing the reactivity of the edge atoms. Our study develops an explanation for the chirality enrichment in the carbon nanotube growth on alloy catalyst particles.

Keywords: Catalysis, Carbon Nanotubes, Alloy Catalyst, Growth Dynamics

*To whom correspondence should be addressed

[†]Fachbereich Physik, Freie Universität Berlin, 14195 Berlin, Germany

[‡]Department of Engineering, University of Cambridge, Cambridge CB2 1PZ, United Kingdom

Introduction

Carbon nanotubes have mechanical and electrical properties, depending on the helicity/atomic structure of the carbon atoms on their tubes surface (chirality).¹⁻³ The self assembling growth process of nanotubes generates nanotubes with various chiralities in the same growth ensemble.⁴ Three phases have been suggested to account for the chirality distribution found in nanotube ensembles, the nucleation phase,⁵ the growth phase,^{6,7} and the termination of the growth.⁸ The nucleation phase involves the formation of graphene-like sheets (sheets of hexagonally arranged carbon atoms) which need to have pentagons in their structure to induce curvature.⁹ Only with the curvature, which is achieved by a curved template particle, it is possible for a graphene sheet to transform into a carbon nanotube cap and lift off the particle.^{10,11} This cap can then elongate with a chirality dependent growth rate by carbon addition to the edge of the growing tube.^{6,7,12} Many theoretical and experimental studies tried to understand how the self assembly of nanotubes works, however, it is still not fully understood how the chirality can be controlled during the growth of carbon nanotubes.^{5,6,9,12-19}

In recent experimental studies it was found that growth on alloy NiFe particles leads to an enrichment of certain chiralities.^{20,21} A theoretical study on a nickel particle suggested that the electronic charge transfer might be important to control the chirality-selective growth process.²² Another theoretical study attempted to explain the chirality enrichment on the NiFe alloy particles by the lower excess energies for certain chiralities.²³ The study, however, considered plane surfaces and elongated nanotube caps (non-minimal seed caps with only an inferior number of growth sites/kinks), which does not seem to be appropriate to describe the chirality selection on a catalyst particle.^{23,24}

In this paper we study the (5, 5) armchair and (9, 0) zigzag carbon nanotube caps connected to various Ni, NiFe and Fe catalyst particles. We calculate the average carbon-metal bond energies, adhesion energies and charge distributions using density functional theory. We find the highest adhesion and lowest excess energy for armchair and zigzag caps on the Ni₂₇Fe₂₈ alloy cluster. Small energy differences between the armchair and zigzag bonds allow to derive carbon addition barriers.

The barriers can be used in a growth model leading to chirality distributions that compare satisfactorily with the recent experimental results of growth on NiFe alloy particles. A charge transfer from the catalyst particles to the caps induces a dipole moment between the catalyst particle and the cap. The polarity of the bond between the cap edge and catalyst atoms increases with increasing Fe content. The charge redistribution is found to depend on the chirality, as the line density of edge sites increases with higher chiral angle. The excess electron charges on the armchair rim atoms are found to be between (2.90 ± 0.06) e for Ni and (4.15 ± 0.14) e for Fe. The increasing reactivity induced through the excess electron charges on the edge carbon cap atoms allows to explain why the nanotube growth rate on iron is higher than on nickel.

Methodology

Computational Methods

We performed spin polarized density functional theory calculations with the *ab-initio* package SIESTA.^{25,26} We used the generalized gradient approximation parameterized by Perdew, Burke and Ernzerhof,²⁷ as the bias towards compact cluster structures is reduced compared to the local density approximation.²⁸ The calculations used norm conserving nonlocal pseudopotentials generated in the scheme of Troullier and Martins with the parameters presented in the PhD thesis of Dumlich.^{24,29} The valence electrons were described by localized pseudoatomic orbitals. To balance the computational time and the accuracy to a reasonable level, we used a double- ζ polarized (DZP) basis set. The cutoff radii of the orbitals were chosen with $r_s = 6.099$ Bohr and $r_p = 7.832$ Bohr for the *s* and *p* orbital of the carbon atoms, $r_s = 9.649$ Bohr and $r_d = 6.001$ Bohr for the *s* and *d* orbital of the iron atoms, and $r_s = 9.187$ Bohr and $r_d = 5.572$ Bohr for the *s* and *d* orbital of the nickel atoms. The mesh-cutoff for the real-space integration corresponded to about 350 Ry. We used only the Γ -point to calculate the total energies, as all studied systems have finite dimensions.

For our calculations we consider the situation, in which a carbon nanotube cap has already

formed on a catalyst particle, but is not elongated. The systems studied in this paper therefore consist of two parts, a catalytic particle and a carbon nanotube cap. We consider the Fe_{55} , $\text{Ni}_{12}\text{Fe}_{43}$, $\text{Ni}_{27}\text{Fe}_{28}$, and Ni_{55} clusters to understand the influence of alloy systems and chiralities on the cap-cluster interaction.

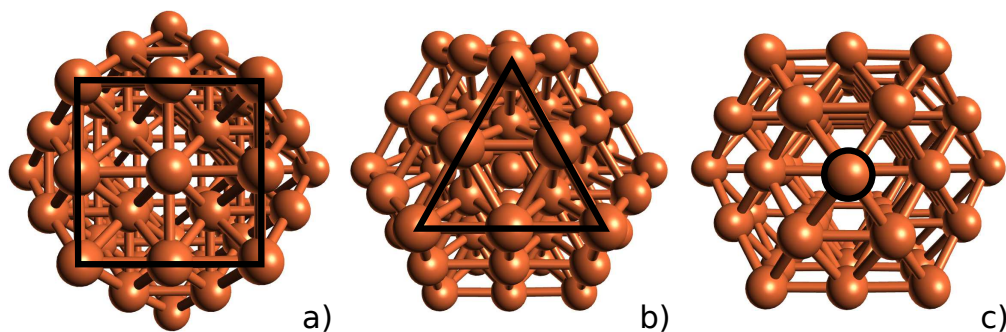


Figure 1: Top view on a ball and stick sketch model of the spots of a 55 atom (iron) cluster. The atoms that form the top of the cluster are marked. a) Spot 1, fcc(100) with a 3 times 3 atom *square* (9 atoms). b) Spot 2, fcc(111) with a 3 atom sided *triangle* (6 atoms). c) Spot 3, with only 1 atom at the *top* of the cluster.

Our (deformed) icosahedral catalyst particles consists of 55 atoms³⁰ that initially form a highly symmetric structure containing six fcc(100), eight fcc(111) surfaces, and three distinctive spots to add a carbon nanotube cap, see 1 a) to 1 c). The icosahedral particles have been found to be the most stable configuration.³⁰ The relaxed particle structures do not keep the icosahedral symmetry and are not expected to represent the global minimum, as it is not feasible to find the global minimum of the clusters in density functional theory.^{28,31} The energy differences between different geometry optimized catalyst clusters range between 2 eV and 3 eV, corresponding to previously reported values.³¹ We calculated the energies of the geometry optimized catalyst structures from each individual initial structure of the combined system to derive consistent carbon-metal and adhesion energies.

The carbon nanotube caps were created with the program code CaGe using the isolated pentagon rule (IPR), which states that caps are energetically most stable, if all six pentagons needed for the cap inclination are isolated from each other.³²⁻³⁴ We created and geometry optimized fullerene structures starting from the as-generated caps of CaGe to get to a decent cap structure. There are

many cap configurations for a certain chirality, which hinders to draw conclusions for the most chiralities.^{33,34} The isolated pentagon rule used for the generation of our caps, however, allows to reduce the number of possible caps, by only considering energetically favorable structures.³⁴ Especially the (5,5) (30 atom cap) and (9,0) (39 atom cap) chiralities only have one possible cap structure which fulfills the isolated pentagon rule,³⁵ making them perfect candidates for our study.

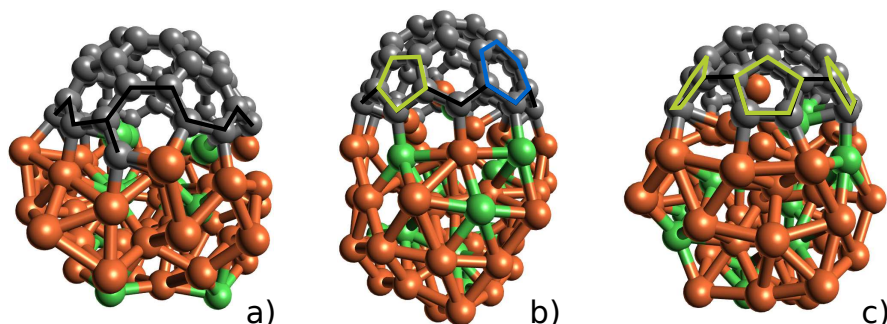


Figure 2: Ball and sticks sketch model of carbon nanotube caps on a $\text{Ni}_{12}\text{Fe}_{43}$ alloy cluster on three different spots. Carbon atoms in grey, nickel atoms in green, and iron atoms in orange. (a) Spot 1: (9,0) cap shows a Klein-edge through bond break of a pentagon at the rim. (b) Spot 2: (9,0) cap showing a hexagon and pentagon at the zigzag rim. (c) Spot 3: (5,5) cap showing an armchair rim formed exclusively by pentagons.

The caps were transferred on the three different spots of the catalyst particles, see 1. The fit of the rims of the carbon nanotube caps to the spots of the clusters were performed by hand. In 2 we show geometry optimized structures of the (9,0) and (5,5) cap bound to the three spots of the $\text{Ni}_{12}\text{Fe}_{43}$ catalyst as examples for all the systems we studied. The atoms at the rim of the cap bind to the cluster, see 2. The deformation (structure change) of the cluster is significant for the presented alloy systems. The atoms in the rim of the cap also adjusted their positions, which suggests a dynamic process of carbon and metal reshaping.^{36,37} The edges/rims of the caps are composed of only armchair and zigzag sites, which is true for all nanotubes. If a pentagon bond gets broken at the edge, a Klein-edge can form and offer a site for addition of a single carbon atom to close the edge with a hexagon, see 2 a). The Klein-edge configuration occurs commonly for the (9,0) cap on the *square* spot and for the (5,5) cap on the *top* spot and might be a possible way to avoid the initiation barrier for a new layer. The configuration with the Klein edge was recently

suggested to be energetically favorable for the armchair growth of graphene (A5' site).³⁸ In general there is a nearly continuous number of ways to combine the cap with the cluster in dependence of the chirality of the cap, however, the chosen spots are expected to allow for the best comparison.

All optimized geometries were relaxed to a maximal atomic force of 0.04 eV/Å. The total energy of the combined system as well as the energy of the cluster and cap were calculated in various structures and basis sets to account for the basis set superposition error (counterpoise correction).^{39–42} The basis set superposition errors for our calculations range between 2.0 eV and 3.0 eV with an average error of (2.5 ± 0.3) eV. The adhesion energy between the carbon nanotube cap and the catalyst cluster can be calculated with:

$$E_{ad} = E_{tot} - E_{cap}^{relax} - E_{cluster}^{relax} - E^{BSSE}, \quad (1)$$

where E_{tot} is the energy of the geometry optimized combined system of the cap and the catalyst cluster, E_{cap}^{relax} is the energy of the geometry optimized cap, and $E_{cluster}^{relax}$ is the energy of the geometry optimized cluster.^{31,43}

To assess the stability of the combined system we compare the cap-on cluster system with other systems that contain the same number of carbon and metal atoms. This leads to formulas for the excess energy:

$$E_x^i = E_{tot} - E_{cluster}^{relax} - n_C E_C^i - E^{BSSE}, \quad (2)$$

with E_C^i the energy per carbon atom for the system the combined cap-on-cluster system is compared to and n_C the number of carbon atoms in the cap of the combined system.^{5,31,44} We calculate the excess energy per atom in comparison to the energy of a system of an isolated metal cluster and a fullerene, to determine which system configuration is lower in energy and therefore more stable.^{5,31,44} Alternatively the excess energy compared to the fullerene structure can be obtained by removal of the dangling bond contributions of the adhesion energy. This leads to

$$E_x^{fullerene} = E_{CM} = E_{ad} - 2 \cdot m \cdot E_a^{vac} - (n - m) \cdot E_z^{vac}, \quad (3)$$

where E_{ad} is the adhesion energy, E_a^{vac} is the armchair bond energy in vacuum, and E_z^{vac} is the zigzag bond energy in vacuum. The factor $2 \cdot m$ results from the number of armchair bonds at the rim of the nanotube cap and the factor $(n - m)$ results from the number of zigzag bonds at the rim of the cap.^{7,45} The vacuum bond energies (for a straight cut rim) can be derived with the equations $E_a^{vac} = \frac{E_{C_{60}}/2 - E_{cap}^{(5,5)}}{2 \cdot m}$ and $E_z^{vac} = \frac{E_{C_{78}}/2 - E_{cap}^{(9,0)}}{n - m}$ where E_{C_i} is the energy of a fullerene formed from two (n, m) caps. We used the system specific vacuum bond energies to determine the carbon-metal bond energies. To determine the carbon-metal bond energies per bond we divided through the number of bonds at the edge $n + m$.

An error for the energies was estimated from the standard deviation by averaging over identical systems with small changes in their initial configuration. The standard deviations are rather large, as only two values were included which does not have a statistical significance, however, it allows to estimate the order of the error with at least 0.1 eV for the excess energy. The error for the adhesion energy is estimated to be slightly higher with about 0.7 eV.

We performed Bader population analysis calculations on the cap-cluster systems to determine the electron charge transfer between the carbon cap atoms and the catalyst particle atoms.⁴⁶⁻⁴⁹

Growth model

The growth model applied in this paper is based on the idea that the carbon addition occurs to the hexagonal rim of the nanotube.^{7,45} The hexagonal rim contains armchair and zigzag edges.^{7,45} The addition of carbon dimers elongates the rim with hexagons and transforms the rim through a change of the number of energetically favorable addition sites.^{7,45} An energy barrier occurs for the addition of carbon atoms to the rim, which is especially high for the addition to zigzag rims.^{6,7} The energy barrier for the rim transformation occurring through the carbon dimer addition to an armchair rim (initiation/closing of a new layer) is determined by

$$\Delta_a = 2 \cdot |E_z - E_a|, \quad (4)$$

where E_a is the energy of an armchair carbon-metal bond and E_z is the energy of a zigzag carbon-metal bond.^{7,24} The energy barriers influence the chirality dependent growth rate.^{6,7,12} A factor for the different growth rates in dependence of the chirality is given with

$$\Gamma(n, m) = \begin{cases} \frac{\Lambda_{aa,aa}(n, m) \cdot \delta_a + \Lambda_{aa,z}(n, m) \cdot \delta_{az}}{n+m} & \text{if } 2m - n > 0, \\ \frac{\Lambda_{aa,z}(n, m) \cdot \delta_{az}}{n+m} & \text{otherwise,} \end{cases} \quad (5)$$

where $\delta_a = \exp(-\Delta_a/k_b T)$ is an exponential factor to account for the temperature dependence of the addition barrier to armchair sites and $\delta_{az} = \exp(-\Delta_{az}/k_b T) = 1$, as an addition barrier for $aa.z$ sites (kinks) is negligible ($\Delta_{az} = 0$).^{6,7,24} The other terms are defined as $\Lambda_{aa,aa} = 2m - n - 1 + 1/(2m - n)$ and $\Lambda_{aa,z} = \min(m, n - m)$.⁷ The growth rate factor $\Gamma(n, m)$ can have values between 0 and 0.5 in dependence of the chirality.

$\Gamma(n, m)$ allows to determine the relative difference in growth rate between different chiralities. To derive a chirality distribution we include the influence of the nucleation phase, i.e., whether a particular tube cap is nucleated or not.³⁴ We assume the tube diameters (and also the chirality) to be fixed by the nucleation.^{5,50} To consider the dependence of nanotube diameters on the diameter of the catalyst particles,⁵¹⁻⁵³ we therefore multiply Equation (??) by a Gaussian distribution of the nanotube diameters $f(d; \mu, \sigma^2)$ and obtain a growth rate factor $\Gamma^*(n, m)$ which can be compared to a chirality distribution,

$$\Gamma^*(n, m) = \frac{1}{\sigma\sqrt{2\pi}} e^{-\frac{(d-\mu)^2}{2\sigma^2}} \cdot \Gamma(n, m). \quad (6)$$

The tube diameter distribution might also include additional effects that do not result from the particle diameters and which might not be covered by the Gaussian distribution, however, the distribution serves the simplicity of the model.

Results

Adhesion energies and carbon-metal bond energies of nanotube caps

The adhesion energies are high with slightly more than -20 eV, varying about a few eV in dependence of the spot, catalyst and cap. Therefore the nanotube caps are not expected to lift off the catalyst particle spontaneously and perform dome closure.^{54,55} The armchair caps have adhesion energies that are a few eV higher than the zigzag energies, which is a result of the number of dangling bonds at the edge of the caps. The zigzag caps have $n + m = 9 + 0 = 9$ dangling bonds. The armchair caps have $n + m = 5 + 5 = 10$ dangling bonds. Therefore the adhesion energy of the armchair cap is higher than the adhesion energy of the zigzag cap, even though the energy per dangling bond is lower for the armchair compared to the zigzag bond.⁵⁵

Table 1: Comparison of adhesion energies and carbon-metal bond energies of nanotube caps on metallic/alloy clusters in eV. The errors are standard deviations from averaging over the spots.

cap	particle	E_{ad} (eV)	E_{CM}/bond (eV)	E_{CM} (eV)
(5,5)	Fe ₅₅	(-21.2 ± 0.0)	(0.43 ± 0.00)	4.3
(5,5)	Ni ₁₂ Fe ₄₃	(-23.2 ± 1.1)	(0.30 ± 0.11)	3.0
(5,5)	Ni ₂₇ Fe ₂₈	(-23.5 ± 1.0)	(0.27 ± 0.07)	2.7
(5,5)	Ni ₅₅	(-23.2 ± 0.3)	(0.32 ± 0.03)	3.2
(9,0)	Fe ₅₅	$(-20.7 \pm -.)$	$(0.40 \pm -.)$	3.6
(9,0)	Ni ₁₂ Fe ₄₃	(-21.2 ± 0.9)	(0.33 ± 0.10)	3.0
(9,0)	Ni ₂₇ Fe ₂₈	(-21.5 ± 1.1)	(0.30 ± 0.13)	2.7
(9,0)	Ni ₅₅	(-20.2 ± 0.0)	(0.46 ± 0.00)	4.1

Averaging the adhesion energies for the alloy compositions we find $E_{ad}^{\text{Fe}_{55}} = (-21.0 \pm 0.3)$ eV, $E_{ad}^{\text{Ni}_{12}\text{Fe}_{43}} = (-22.3 \pm 1.4)$ eV, $E_{ad}^{\text{Ni}_{27}\text{Fe}_{28}} = (-22.3 \pm 1.5)$ eV, and $E_{ad}^{\text{Ni}_{55}} = (-22.4 \pm 1.5)$ eV. Two effects account for the adhesion energy. One is the structure and the other is the material. The mixture of two materials distorts the catalyst structure as they have different electronic structure resulting in different bond lengths and lattice constants. We observe an increase of adhesion energy for the NiFe alloy systems compared to the pure Fe clusters, see 1, the effect, however, is not

significant.

The adhesion energies averaged on the three spots introduced in 1, show no obvious trend either, with $E_{ad}^1 = (-22.0 \pm 1.5)$ eV for the *square* spot 1, $E_{ad}^2 = (-23.0 \pm 1.4)$ eV for the *triangle* spot 2, and $E_{ad}^3 = (-21.7 \pm 1.0)$ eV for the *top* spot 3. We use this result and average over different spots when calculating adhesion energies as a function of the cap and alloy composition, see 1. The *triangle* spot shows the highest adhesion energy, but the adhesion energies calculated for the other spots are within the standard deviation of spot 2.

The excess/carbon-metal bond energies decrease non monotonically with increasing Ni content from Fe to Ni. The Ni cluster shows the highest excess energy for the (9,0) cap. The lowest excess energy is observed for the Ni₂₇Fe₂₈, which also showed the highest adhesion energy, suggesting that the Ni₂₇Fe₂₈ alloy cluster yields the best growth conditions for the systems compared in this study. The low excess energy allows for a fast formation of caps on the Ni₂₇Fe₂₈ cluster and the higher adhesion energy prevents the cap lift off, which makes the NiFe alloy systems more stable compared to the pure elemental catalyst clusters.

Charge distribution on cap and cluster atoms

Table 2: Charge redistributions between the carbon nanotube caps and the metallic/alloy clusters. q_C^{rim} is the total charge shift of the carbon atoms at the rim of the nanotube cap, q_C is the total charge shift considering all carbon atoms of the cap, q_{Fe} is the total charge shift considering all iron atoms, and q_{Ni} is the total charge shift considering all nickel atoms of the catalyst particle.

cap	particle	q_C^{rim} (e)	q_C (e)	q_{Fe} (e)	q_{Ni} (e)
(5,5)	Fe ₅₅	(4.15 ± 0.14)	(5.31 ± 0.72)	(-5.32 ± 0.72)	
(5,5)	Ni ₁₂ Fe ₄₃	(4.08 ± 0.31)	(5.06 ± 0.52)	(-7.18 ± 0.65)	(2.12 ± 0.46)
(5,5)	Ni ₂₇ Fe ₂₈	(3.67 ± 0.24)	(4.36 ± 0.36)	(-6.46 ± 0.20)	(2.10 ± 0.32)
(5,5)	Ni ₅₅	(2.90 ± 0.06)	(3.32 ± 0.36)		(-3.33 ± 0.38)
(9,0)	Fe ₅₅	(3.26 ± -.)	(4.68 ± -.)	(-4.68 ± -.)	
(9,0)	Ni ₁₂ Fe ₄₃	(3.39 ± 0.17)	(4.62 ± 0.22)	(-6.71 ± 0.42)	(2.09 ± 0.59)
(9,0)	Ni ₂₇ Fe ₂₈	(2.99 ± 0.05)	(3.96 ± 0.02)	(-6.48 ± 0.29)	(2.52 ± 0.28)
(9,0)	Ni ₅₅	(2.34 ± 0.08)	(3.11 ± 0.42)		(-3.11 ± 0.42)

The charge population on the atoms in the rim of the cap and for the metal atoms in the catalyst particle shows a stronger trend than the energies, see 2. All charge values are excess charges compared to the isolated atom valence electron configuration with 8 charges on each Fe atom, 10 charges on each Ni atom and 4 charges on each C atom. The metal atoms partly loose their electrons to the carbon atoms in the cap, with whom they form carbon-metal bonds. The amount of electron charge transfer to the carbon atoms depends on the catalyst element and on the bond type of the edge atom (zigzag or armchair). The charge on the rim of the armchair cap is higher than on the rim of the zigzag cap. The trend weakens, but does not vanish, if the charge transfer per bond is considered, as the number of carbon-metal bonds is 10 for the armchair and only 9 for the zigzag cap. Considering the charge transfer to the whole cap and dividing through the number of bonds leads to an equal charge transfer to the armchair and zigzag caps per bond. The highest layer of the catalyst atoms supplies the major part of the electrons to the carbon nanotube cap. The carbon atoms of the cap that are not part of the rim have an average valence charge of about 4 e, with low deviations (below 0.1 e), which means that they do not take part in the charge redistribution/polar binding between the metal catalyst and the carbon cap. The electron charge redistribution is localised at the outer rim atoms of the cap that form the carbon-metal bonds, corresponding to a polar bond. The localisation is slightly higher for the armchair edges with about 80% of the charge localised at the outer rim atoms compared to about 74% at the outer edge zigzag cap atoms, which is the reason why the armchair rim atoms yield a higher charge per bond.

The charge on the cap increases with Fe content and becomes maximal for the elemental Fe cluster. We observe the same behaviour at the rim, with the exclusion of the (9,0) cap on Fe, which, however, may be an artifact, as only one cap was considered on spot 3. The higher charge points to a higher reactivity on Fe compared to Ni, which likely leads to a faster growth rate on iron compared to nickel, previously observed experimentally.⁵⁶

The Fe atoms do not only supply their electron charge to the C atoms, but also to the Ni atoms, see the charge transfer for the NiFe alloy systems in 2. The iron atoms loose about 5-7 electron charges. The nickel atoms either gain about 2-2.5 e in the alloy systems or loose about 3 e if Ni

is the only element in the catalyst particle. The carbon atoms in the cap always receive electron charges, see 2. The total amount of charge received by the carbon cap is about 3-5 e. The amount of charge supplied to the rim is slightly lower with about 2-4 e.

Following from the reactivity argument, which results from the increased charge on the edge atoms, we can give a geometric argument for the preference of armchair over zigzag structures in the following. It follows from the number of edge sites. We consider the line density of edge sites, which corresponds to the number of edges sites divided by the circumference of the nanotube rim

$$\lambda = \frac{N_a + N_z}{|\vec{C}_h|} = \frac{n + m}{a_0 \cdot \sqrt{n^2 + nm + m^2}}, \quad (7)$$

with $N_a + N_z$ the number of armchair and zigzag sites and $|\vec{C}_h|$ the circumference of the tube. The rightmost equation follows for straight rim configurations. Equation (7) leads to a line density of $\lambda_a = 2/(\sqrt{3}a_0)$ for ($n = m$) armchair and $\lambda_z = 1/a_0$ for (n integer, $m = 0$) zigzag tubes, for all other tubes ($n \neq m \neq 0$) the value of the line density is between λ_a and λ_z ($\lambda_a > \lambda_c > \lambda_z$). Considering the fact that a higher density of edge sites increases the number of carbon metal bonds, directly gives the argument why armchair tubes are preferred compared to zigzag tubes, as the number of electrons at the edge is increased, yielding a higher reactivity. The comparison of the (5,5) cap to the (9,0) cap presented here, serves as an example as they have nearly identical diameters, but a different number of edge sites. The increased number of sites with higher chiral angles leads to an enrichment of armchair/near-armchair tubes in nanotube samples from simple geometric reasoning. This geometric argument might also be translated to growth rate considerations of nanotubes. The edges of tubes with higher chiral angles contain more sites for carbon atoms to dock, independent of the exact addition mechanism, supporting arguments for faster growth of higher chiral angle tubes.

The charge transfer also induces a dipole moment in the nanotube cap and cluster system, see 3. The highest electric dipole moment can be found with 14.7 Debye for the (9,0) cap on spot 3 of the Fe cluster and the lowest electric dipole moment is 7.4 Debye for the (5,5) cap on the Ni cluster.

Table 3: Electric dipole moments Δ between the nanotube caps and metallic clusters in Debye. The last column of the table shows electric dipole moments for the armchair/zigzag caps averaged over the spots of a specific catalyst composition.

cap	particle	Δ_{avg} (Debye)
(5,5)	Fe ₅₅	12.4
(9,0)	Fe ₅₅	14.7
(5,5)	Ni ₁₂ Fe ₄₃	10.6
(9,0)	Ni ₁₂ Fe ₄₃	12.1
(5,5)	Ni ₂₇ Fe ₂₈	10.0
(9,0)	Ni ₂₇ Fe ₂₈	11.4
(5,5)	Ni ₅₅	8.6
(9,0)	Ni ₅₅	9.7

A decrease of the electric dipole moment is correlated with the Ni content in the composition of the catalyst particle, where higher Ni content leads to lower electric dipole moments. The zigzag caps have higher electric dipole moments compared to the armchair caps, which is likely a result of the weaker localisation of electron charge at the carbon-metal bond forming atoms for the zigzag caps. The difference of the average electric dipole moments of a certain catalyst composition between armchair and zigzag caps decreases with increasing Ni content, with the highest difference of 2.3 Debye on Fe and the lowest difference of 1.1 Debye on Ni. The electric dipole moments generate an electric field, which was suggested to increase the landing probability of carbon atoms on the catalyst particle.⁵⁷ Therefore the landing probability on Fe is higher than on Ni, leading to a higher growth rate on catalysts containing Fe. A higher landing probability might also become a problem, if the carbon atoms cannot be incorporated at the edge faster than the carbon precursors land on the particle, as this might lead to amorphous carbon encapsulation of the catalyst and prevent further growth. The higher landing probability for zigzag caps can lead to a reduced number of zigzag tubes, as zigzag edges are expected to have a slower growth rate, which makes it especially hard to fulfill the requirement of fast carbon incorporation to prevent catalyst encapsulation.

Discussion

In the following we want to discuss the results we can derive from the energies and charge distributions calculated in this paper and compare them to other studies. There are two important results, that can be derived from the carbon-metal bond energies. First, the energies are important for the nucleation phase, as lower excess (carbon-metal bond) energies point to a higher formation probability.^{5,58} Second, the carbon addition barrier Δ_a can be derived from the carbon-metal bond energies for the growth phase, which was found to influence the chirality dependent growth rate.^{6,7,12} Both phases determine the chirality of the carbon nanotube ensemble which is grown during the nanotube synthesis. We determine the barrier energies Δ_a (Equation (??)), by using $E_a = E_{CM}^{(5,5)}/\text{bond}$ and $E_z = E_{CM}^{(9,0)}/\text{bond}$ of 1. The barriers result from small deviations between armchair and zigzag bond energies. Previous studies considered flat metallic surfaces as catalysts and tried to optimize the fit between the catalyst surface and the edge of the cap.^{5,23} On a curved particle, as in this paper, a perfect fit between the edge of the nanotube cap and the catalyst particle is not possible, which increases the carbon-metal bond energies. The bond energies for armchair edges from Reich *et al.*, derived for a flat Ni surface, range from $E_a = 0.12$ eV to $E_a = 1.12$ eV, comparing well to our average value $E_a^{\text{Ni}_{55}} = (0.32 \pm 0.04)$ eV.⁵ The values for zigzag edges from Reich *et al.* range from $E_z = 0.16$ eV to $E_z = 1.44$ eV, which are also comparable to our value $E_z^{\text{Ni}_{55}} = 0.46$ eV.⁵ The caps connect to various spots on the catalyst clusters which increases the deviation of the bond energies and therefore renders the chiral selectivity by structural fit of the cap and the catalyst particle unlikely. The large standard deviations point to a general problem for *ab-initio* studies of carbon nanotube growth. The quantitative reproducibility is rather weak and it should be desired to test various systems with slightly different configurations/parameters. The energy barriers for the studied catalyst compositions are calculated with $\Delta_a^{\text{Fe}_{55}} = 0.06$ eV, $\Delta_a^{\text{Ni}_{12}\text{Fe}_{43}} = 0.06$ eV, $\Delta_a^{\text{Ni}_{27}\text{Fe}_{28}} = 0.06$ eV, and $\Delta_a^{\text{Ni}_{55}} = 0.28$ eV. The barriers are equal for all iron containing catalyst compositions.

The barriers can be inserted in Equation (??) to determine the chirality distributions, where the contribution of $\Gamma(n, m)$ (Equation (??)) is equal for all systems that mainly contain iron atoms

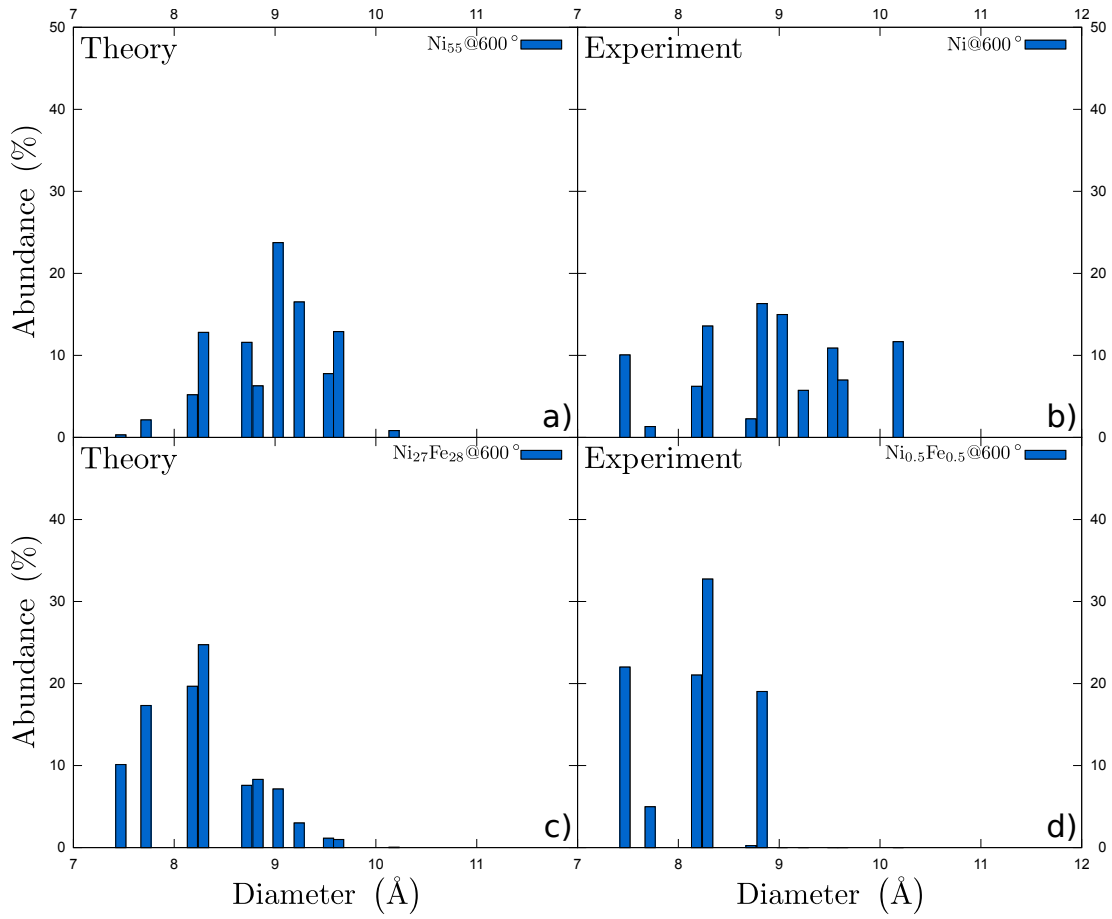


Figure 3: Normalized abundances in dependence of the tube diameter; a) ($\mu = 9.0 \text{ \AA}$, $\sigma = 0.6 \text{ \AA}$) and c) ($\mu = 8.1 \text{ \AA}$, $\sigma = 0.6 \text{ \AA}$) estimated from our theoretical growth model, see Equation (??); b) and d) from experimental photoluminescence data by Chiang *et al.* for nanotubes grown on Ni and on a nickel-iron alloy at 600° C .²⁰

$(\delta_a = 0.45$ for $600^\circ\text{C})$ and only the gaussian diameter distribution factor changes the chirality distribution. We can compare the results of our model to the experimental results presented by Chiang *et al.*, who grew nanotubes on NiFe alloy systems to analyse the influence of the catalyst composition on the chirality distribution of a nanotube ensemble.^{20,21} They derived chirality distributions from photoluminescence data using calculated photoluminescence intensities.^{20,59} The chirality distributions satisfactorily fit the results derived from our growth model, see 3.²⁰ Especially the growth on iron containing systems is interesting, as the experimental study found the chirality distributions grown from catalyst with the composition $\text{Ni}_{0.27}\text{Fe}_{0.73}$ and $\text{Ni}_{0.5}\text{Fe}_{0.5}$ to be almost identical,²⁰ corresponding well to our results. The Ni catalyst particle has a significantly larger barrier energy, leading to a suppression of armchair growth sites, as, e.g. $\delta_a = 0.024$ for 600°C . In the experimental study the nanotubes grown on a Ni catalyst show a relatively wide chirality distribution with a peak for (9,4).^{20,21} Especially important seems to be the diameter region of the nanotubes with 9.0 \AA for (9,4) and 8.8 \AA for (7,6) which have the highest intensity/abundance in the experimental study.²⁰ A slight descent of intensity occurs for chiralities with diameters that have smaller/higher tube diameters than about 9.0 \AA , pointing to a lower number of catalyst particles, or other unknown effects, to grow tubes of that higher/lower diameters. Increasing the iron content of the composition of the catalyst particles until iron becomes the major component, leads to a significant narrowing of the chirality distribution to only a few chiralities at lower diameters, compared to the Ni catalyst particle, see 3 d). The fcc-lattice constant of iron $a_{\text{Fe}} = 3.45\text{ \AA}$ is lower than the lattice constant of nickel $a_{\text{Ni}} = 3.63\text{ \AA}$,⁶⁰ which leads to smaller diameter alloy catalyst particles with increasing Fe content, which might be a reason for the shift of the chirality distribution to lower diameter nanotubes ((7,6) and (8,4) abundance increased), as the diameter of the grown nanotubes depend on the diameter of the catalyst on which they are grown in the tangential growth mode/under growth conditions close to thermodynamic equilibrium.^{51–53} The experimental study, however, tried to obtain equal particle diameters through the preparation process, pointing to a dependence on the material instead of the catalyst diameters.²⁰ Our model was not intended to perfectly reproduce all abundances, however, it still gives a fair approximation

to the experimental results and successfully reproduces the most significant change in the chirality distribution by the change of the catalyst.

Besides the chirality distributions obtained from our growth model we also want to compare our charge transfer results to the literature. Wang *et al.* suggested that the short ranged charge distribution on nanotube edge atoms and catalyst atoms might be important for the chirality-selective growth of carbon nanotubes, as electron charges would increase the reactivity of the edge atoms.²² We observe an increase of electron charge on the carbon edge atoms with charge supply by the metal atoms in agreement with Wang *et al.*²² The average charge values on the carbon rim atoms, see 2, compare well to the values calculated by Wang *et al.* for, e.g., the (5,5) nanotube cap on nickel we find an average value of 0.29 e which compares to the slightly higher values of Wang *et al.* between 0.31 e and 0.38 e. To determine the effect of the charges on chirality distributions, we also put a focus on alloy systems. In alloy systems a charge distribution between two metallic species leads to an electron accumulation not only on the carbon edge atoms, but also on the nickel atoms. We find higher charges on armchair than on zigzag edges, which was suggested by Wang *et al.* to be used to influence the chirality.²² The alloy composition has a significant effect on the charge distribution. We find an increase of electron charge on the carbon cap edge atoms from Ni to Fe with increasing Fe content in the alloy, pointing to an increased growth rate of nanotubes through increased reactivity of the nanotube edge atoms, which compares well to the higher growth rates found for iron compared to nickel.⁵⁶ Another relevant factor for the growth rate was found to be the metal d orbital energy.⁶¹ The charge distribution patterns suggested by Wang *et al.* resemble the edge structure of armchair and zigzag sites.

Theoretical studies can only model some aspects of the nanotube growth, neglecting other aspects, e.g., the effect of Ostwald ripening,⁸ that influence the chirality distribution as well. Further the chirality distributions determined in experiments have to be regarded with care as huge differences for the abundances of the chiralities might arise through the method used to determine the abundances, i.e. the intensity of a measured entity is not directly proportional to the abundance of the tube.^{59,62,63} Therefore we did not expect to obtain results that perfectly match our growth

model, however, we see it as a success that the model correctly describes the qualitative features of the chirality selective growth process, which suggests, that the model might include some part of the truth to solve the puzzle of chirality selective growth.

Conclusions

In summary we calculated adhesion energies, excess energies, and electronic charge redistributions between carbon nanotube caps and NiFe alloy systems using density functional theory. The highest adhesion energies and lowest excess energies are found for the Ni₂₇Fe₂₈ alloy cluster, for both armchair and zigzag caps. The energy differences between armchair and zigzag were found to be low. The curved form of the catalyst particle can be regarded as a constraint to the fit between the nanotube edge and the catalyst, which tends to lower the energy difference between armchair and zigzag caps. The small energy differences between the armchair and zigzag caps allow to derive carbon addition barriers, which - using the growth model presented in this paper - lead to chirality distributions that compare satisfactorily with experimental results. The charge transfer between the cap and the catalyst particles increases with increasing Fe content, which induces a dipole moment. The charge transfer to the armchair caps is higher than to the zigzag caps, in contrast to the electric dipole moment, which is higher for zigzag than for armchair caps and has a maximum of about 15 Debye on the iron particle. This is a consequence of the chirality dependent line density of edge sites, which decreases with lower chiral angle. The excess electron charges on the carbon rim atoms increase with Fe content of the catalyst particle from (2.90 ± 0.06) e for Ni to (4.15 ± 0.14) e for Fe. The excess electron charges increase the reactivity of the carbon cap atoms, which explains why the nanotube growth rate on iron is higher than on nickel. Our results will be useful for the understanding of the growth of carbon nanotubes on alloy catalysts.

Acknowledgement

We acknowledge S. Heeg and M. Fouquet for useful discussions. This work was supported by ERC under grant no. 210642.

References

- (1) Reich, S.; Thomsen, C.; Maultzsch, J. *Carbon Nanotubes*; Wiley VCH: Berlin, Germany, 2003, Ch. 2.
- (2) Saito, R.; Fujita, M.; Dresselhaus, G.; Dresselhaus, M. S.; Electronic Structure of Graphene Tubules Based on C60. *Phys. Rev. B* **1992**, 46, 1804-1811.
- (3) Odom, T. W.; Huang, J.-L.; Kim, P.; Lieber, C. M.; Atomic Structure and Electronic Properties of Single-Walled Carbon Nanotubes. *Nature* **1998**, 391, 62-64.
- (4) Bachilo, S. M.; Strano, M. S.; Kittrell, C.; Hauge, R. H.; Smalley, R. E.; Weisman, R. B.; Structure-Assigned Optical Spectra of Single-Walled Carbon Nanotubes. *Science* **2002**, 298, 2361-2366.
- (5) Reich, S.; Li, L.; Robertson, J.; Control the Chirality of Carbon Nanotubes by Epitaxial Growth. *Chem. Phys. Lett.* **2006**, 421, 469-472.
- (6) Ding, F.; Harutyunyan, A. R.; Yakobson, B. I.; Dislocation Theory of Chirality-Controlled Nanotube Growth. *Proc. Natl. Acad. Sci. U.S.A.* **2009**, 106, 2506-2509.
- (7) Dumlich, H.; Reich, S.; Chirality-Dependent Growth Rate of Carbon Nanotubes: A Theoretical Study. *Phys. Rev. B* **2010**, 82, 085421.
- (8) Boerjesson, A.; Bolton, K.; First Principles Studies of the Effect of Ostwald Ripening on Carbon Nanotube Chirality Distributions. *ACS Nano* **2011**, 5, 771-779.

- (9) Ohta, Y.; Okamoto, Y.; Page, A. J.; Irle, S.; Morokuma, K.; Quantum Chemical Molecular Dynamics Simulation of Single-Walled Carbon Nanotube Cap Nucleation on an Iron Particle. *ACS Nano* **2009**, 3, 3413-3420.
- (10) Schebarchov, D.; Hendy, S. C.; Ertekin, E.; Grossman, J. C.; Interplay of Wetting and Elasticity in the Nucleation of Carbon Nanotubes. *Phys. Rev. Lett.* **2011**, 107, 185503.
- (11) GÃşmez-GualdrÃşn, D. A.; McKenzie, G. D.; Alvarado, J. F. J.; Balbuena, P. B.; Dynamic Evolution of Supported Metal Nanocatalyst/Carbon Structure during Single-Walled Carbon Nanotube Growth. *ACS Nano* **2012**, 6, 720.
- (12) Rao, R.; Liptak, D.; Cherukuri, T.; Yakobson, B. I.; Maruyama, B.; In Situ Evidence for Chirality-Dependent Growth Rates of Individual Carbon Nanotubes. *Nat. Mater.* **2012**, 11, 213-216.
- (13) Iijima, S.; Ajayan, P. M.; Ichihashi, T.; Growth Model for Carbon Nanotubes. *Phys. Rev. Lett.* **1992**, 69, 3100-3103.
- (14) Gavillet, J.; Loiseau, A.; Journet, C.; Willaime, F.; Ducastelle, F.; Charlier, J.-C.; Root-Growth Mechanism for Single-Wall Carbon Nanotubes. *Phys. Rev. Lett.* **2001**, 87, 275504.
- (15) Raty, J.-Y.; Gygi, F.; Galli, G.; Growth of Carbon Nanotubes on Metal Nanoparticles: A Microscopic Mechanism from Ab Initio Molecular Dynamics Simulations. *Phys. Rev. Lett.* **2005**, 95, 096103.
- (16) Yazyev, O. V.; Pasquarello, A.; Effect of Metal Elements in Catalytic Growth of Carbon Nanotubes. *Phys. Rev. Lett.* **2008**, 100, 156102.
- (17) Wang, Q.; Ng, M.-F.; Yang, S.-W.; Yang, Y.; Chen, Y.; The Mechanism of Single-Walled Carbon Nanotube Growth and Chirality Selection Induced by Carbon Atom and Dimer Addition. *ACS Nano* **2010**, 4, 939-946.

- (18) Neyts, E. C.; Shibuta, Y.; van Duin, A. C. T.; Bogaerts, A.; Catalyzed Growth of Carbon Nanotube with Definable Chirality by Hybrid Molecular Dynamics-Force Biased Monte Carlo Simulations. *ACS Nano* **2010**, 4, 6665-6672.
- (19) Fouquet, M.; Bayer, B. C.; Esconjauregui, S.; Blume, R.; Warner, J. H.; Hofmann, S.; Schlögl, R.; Thomsen, C.; Robertson, J.; Highly Chiral-Selective Growth of Single-Walled Carbon Nanotubes With a Simple Monometallic Co Catalyst. *Phys. Rev. B* **2012**, 85, 235411.
- (20) Chiang, W.-H.; Sankaran, R. M.; Linking catalyst composition to chirality distributions of as-grown single-walled carbon nanotubes by tuning NixFe1-x nanoparticles. *Nat. Mater.* **2009**, 8, 882-886.
- (21) Chiang, W.-H.; Sakr, M.; Gao, X. P. A.; Sankaran, R. M.; Nanoengineering NixFe1-x Catalysts for Gas-Phase, Selective Synthesis of Semiconducting Single-Walled Carbon Nanotubes. *ACS Nano* **2009**, 3, 4023-4032.
- (22) Wang, Q.; Yang, S.-W.; Yang, Y.; Chan-Park, M. B.; Chen, Y.; Charge Transfer between Metal Clusters and Growing Carbon Structures in Chirality-Controlled Single-Walled Carbon Nanotube Growth. *J. Phys. Chem. Lett.* **2011**, 2, 1009-1014.
- (23) Dutta, D.; Chiang, W.-H.; Sankaran, R. M.; Bhethanabotla, V. R.; Epitaxial Nucleation Model for Chiral-Selective Growth of Single-Walled Carbon Nanotubes on Bimetallic Catalyst Surfaces. *Carbon* **2012**, 50, 3766-3773.
- (24) Dumlich, H.; In *A Path to Monochiral Ensembles of Carbon Nanotubes and their Properties*; PhD Thesis: FU Berlin, 2013.
- (25) Ordejon, P.; Artacho, E.; Soler, J. M.; Self-Consistent Order-N Density-Functional Calculations for Very Large Systems. *Phys. Rev. B* **1996**, 53, R10441.
- (26) Soler, J. M.; Artacho, E.; Gale, J. D.; Garcia, A.; Junquera, J.; Ordejon, P.; Sanchez-Portal,

- D.; The Siesta Method For ab initio Order-N Materials Simulation. *J. Phys.: Condens. Matter* **2002**, 14, 2745-2779.
- (27) Perdew, J. P.; Burke, K.; Ernzerhof, M.; Generalized Gradient Approximation Made Simple. *Phys. Rev. Lett.* **1996**, 77, 3865-3868.
- (28) Baletto, F.; Ferrando, R.; Structural properties of nanoclusters: Energetic, thermodynamic, and kinetic effect. *Rev. Mod. Phys.* **2005**, 77, 371-423.
- (29) Troullier, N.; Martins, J. L.; Efficient Pseudopotentials for Plane-Wave Calculations. *Phys. Rev. B* **1991**, 43, 1993.
- (30) Singh, R.; Kroll, P.; Structural, electronic, and magnetic properties of 13-, 55-, and 147-atom clusters of Fe, Co, and Ni: A spin-polarized density functional study. *Phys. Rev. B* **2008**, 78, 245404.
- (31) Zhu, W.; Börjesson, A.; Bolton, K.; DFT and tight binding Monte Carlo calculations related to single-walled carbon nanotube nucleation and growth. *Carbon* **2010**, 48, 470-478.
- (32) Brinkmann, G.; Delgado Friedrichs, O.; Liskens, S.; Peeters, A.; Van Cleemput, N.; CaGe - a Virtual Environment for Studying Some Special Classes of Plane Graphs - an Update. *MATCH* **2010**, 63, 533-552.
- (33) Brinkmann, G.; Fowler, P. W.; Manolopoulos, D. E.; Palser, A. H. R.; A Census of Nanotube Caps. *Chem. Phys. Lett.* **1999**, 315, 335-347.
- (34) Reich, S.; Li, L.; Robertson, J.; Structure and Formation Energy of Carbon Nanotube Caps. *Phys. Rev. B* **2005**, 72, 165423.
- (35) Li, L.; Reich, S.; Robertson, J.; Modelling the Nucleation and Chirality Selection of Carbon Nanotubes. *Journal of Nanoscience and Nanotechnology* **2006**, 6, 1-8.

- (36) Gomez-Gualdron, D. A.; Zhao, J.; Balbuena, P. B.; Nanocatalyst Structure as a Template to Define Chirality of Nascent Single-Walled Carbon Nanotubes *J. Chem. Phys.* **2011**, 134, 014705.
- (37) Hofmann, S.; Sharma, R.; Ducati, C.; Du, G.; Mattevi, C.; Cepek, C.; Cantoro, M.; Pisana, S.; Parvez, A.; Cervantes-Sodi, F.; In situ Observations of Catalyst Dynamics during Surface-Bound Carbon Nanotube Nucleation. *Nano Lett.* **2007**, 7, 602-608.
- (38) Artyukhov, V. I.; Liu, Y.; Yakobson, B. I.; Equilibrium at the Edge and Atomistic Mechanisms of Graphene Growth. *PNAS* **2012**, 109, 15136-15140.
- (39) Boys, S. F.; Bernardi, F.; The Calculation of Small Molecular Interactions by the Differences of Separate Total Energies. Some Procedures with Reduced Errors. *Molecular Physics* **1970**, 19, 553-566.
- (40) van Duijneveldt, F. B.; van Duijneveldt-van de Rijdt, J. G. C. M.; van Lenthe, J. H.; State of the Art in Counterpoise Theory. *Chemical Reviews* **1994**, 94, 1873-1885.
- (41) Liu, B.; McLean, A. D.; Accurate Calculation of the Attractive Interaction of two Ground State Helium Atoms. *J. Chem. Phys.* **1973**, 59, 4557.
- (42) Liu, B.; McLean, A. D.; The Interacting Correlated Fragments Model for Weak Interactions, Basis Set Superposition Error, and the Helium Dimer Potential. *J. Chem. Phys.* **1989**, 91, 2348.
- (43) Wang, Q.; Wang, H.; Wei, L.; Yang, S.-W.; Chen, Y.; Reactive Sites for Chiral Selective Growth of Single-Walled Carbon Nanotubes: A DFT Study of Ni₅₅ÅC_n Complexes. *J. Phys. Chem. A* **2012**, 116, 11709-11717.
- (44) Fan, X.; Buczko, R.; Puzos, A. A.; Geoghegan, D. B.; Howe, J. Y.; Pantelides, S. T.; Pennycook, S. J.; Nucleation of Single-Walled Carbon Nanotubes. *Phys. Rev. Lett.* **2003**, 90, 145501.

- (45) Dumlich, H.; Reich, S.; Rims of Carbon Nanotubes - Influence of Chirality. *Phys. Status Solidi B* **2010**, 247, 2722-2725.
- (46) Mulliken, R. S.; Electronic Population Analysis on LCAOMO Molecular Wave Functions. I. *J. Chem. Phys.* **1955**, 23, 1833-1840.
- (47) Henkelman, G.; Arnaldsson, A.; Jonsson, H.; A Fast and Robust Algorithm for Bader Decomposition of Charge Density. *Comput. Mater. Sci.* **2006**, 36, 354-360.
- (48) Sanville, E.; Kenny, S. D.; Smith, R.; Henkelman, G.; Improved Grid-based Algorithm for Bader Charge Allocation. *Journal of Computational Chemistry* **2007**, 28, 899-908.
- (49) Tang, W.; Sanville, E.; Henkelman, G.; A Grid-based Bader Analysis Algorithm without Lattice Bias. *J. Phys.: Condens. Matter* **2009**, 21, 084204.
- (50) Reich, S.; Li, L.; Robertson, J.; Epitaxial Growth of Carbon Caps on Ni for Chiral Selectivity. *Phys. Status Solidi* **2006**, 243, 3494-3499.
- (51) Li, Y.; Kim, W.; Zhang, Y.; Rolandi, M.; Wang, D.; Dai, H.; Growth of Single-Walled Carbon Nanotubes from Discrete Catalytic Nanoparticles of Various Sizes. *J. Phys. Chem.* **2001**, 105, 11424-11431.
- (52) Inoue, S.; Kikuchi, Y.; Diameter Control and Growth Mechanism of Single-Walled Carbon Nanotubes. *Chem. Phys. Lett.* **2005**, 410, 209-212.
- (53) Fiawoo, M.-F. C.; Bonnot, A.-M.; Amara, H.; Bichara, C.; Thibault-Pénisson, J.; Loiseau, A.; Evidence of Correlation between Catalyst Particles and the Single-Wall Carbon Nanotube Diameter: A First Step towards Chirality Control. *Phys. Rev. Lett.* **2012**, 108, 195503.
- (54) Lee, Y. H.; Kim, S. G.; Tomanek, D.; Catalytic Growth of Single-Wall Carbon Nanotubes: An Ab Initio Study. *Phys. Rev. Lett.* **1997**, 78, 2393-2396.
- (55) Oh, D.-H.; Lee, Y. H.; Stability and cap formation mechanism of single-walled carbon nanotubes. *Phys. Rev. B* **1998**, 58, 7407-7411.

- (56) Yuan, Q.; Hu, H.; Ding, F.; Threshold Barrier of Carbon Nanotube Growth. *Phys. Rev. Lett.* **2011**, 107, 156101.
- (57) Mohammad, S. N.; A Possible Role of the Dipole Moment of the Catalyst Droplet in Nanotube Growth, Alignment, Chirality, and Characteristics. *Nanotechnology* **2012**, 23, 085701.
- (58) Ding, F.; Larsson, P.; Larsson, J. A.; Ahuja, R.; Duan, H.; Rosen, A.; Bolton, K.; The Importance of Strong Carbon-Metal Adhesion for Catalytic Nucleation of Single-Walled Carbon Nanotubes. *Nano Lett.* **2008**, 8, 463-468.
- (59) Oyama, Y.; Saito, R.; Sato, K.; Jiang, J.; Samsonidze, Ge. G.; Grüneis, A.; Miyauchi, Y.; Maruyama, S.; Jorio, A.; Dresselhaus, G.; Dresselhaus, M.S.; Photoluminescence Intensity of Single-Wall Carbon Nanotubes. *Carbon* **2006**, 44, 873-879.
- (60) Dumlich, H.; In *Growth of Carbon Nanotubes on Catalytic Metal Particles*; Diploma Thesis: FU Berlin, 2009, 19-21.
- (61) Robertson, J.; Heterogeneous Catalysis Model of Growth Mechanisms of Carbon Nanotubes, Graphene and Silicon Nanowires. *J. Mater. Chem.* **2012**, 22, 19858-19862.
- (62) Reich, S.; Thomsen, C.; Robertson, J.; Exciton Resonances Quench the Photoluminescence of Zigzag Carbon Nanotubes. *Phys. Rev. Lett.* **2005**, 95, 077402.
- (63) Heeg, S.; Malic, E.; Casiraghi, C.; Reich, S.; Quantitative Composition of a Single-Walled Carbon Nanotube Sample: Raman Scattering Versus Photoluminescence. *Phys. Status Solidi B* **2009**, 246, 2740-2743.